Wear behaviour of laser cladded Ni-based-WC-La_2O_3 hybrid composite coating on H13 steel at elevated and ambient temperatures

P. Ashtari [1] , N. Parvini Ahmadi [2], S. Yazdani *[3]

Faculty of Materials Engineering, Sahand University of Technology, Tabriz, Iran

Abstract

Hybrid composite coatings have distinct advantages over single composite coatings due to their multipurpose applications. Moreover, nickel-based composite coatings are widely used in corrosive and fatigue environments due to their good wear and corrosion resistance. In this study, NiCoCrAl/tungsten carbide/1-4 wt% lanthanum oxide composite coatings are deposited on H13 hot work tool steel by laser cladding. The wear resistance of the coatings is evaluated when sliding against alumina ball both at room temperature and 700 °C. The results show that the wear rate of the coatings decreases at room temperature by adding 1-3 wt% lanthanum oxide (72.55×10-6 mm^3 N^{-1} m^{-1} for NiCoCrAl/tungsten carbide/2 wt% lanthanum oxide). The coefficient of friction also decreases at this amount of lanthanum oxide and for the samples with 2 and 3 wt% lanthanum oxide, the steady-state of wear starts earlier than the others. At the high temperature of 700 °C, the presence of lanthanum oxide changed the wear mechanism from adhesive to abrasive and improved the wear performance of the coatings. At higher levels of lanthanum oxide, debris removals is observed on the coatings leading to three-body and severe wear.

Keywords: Wear behaviour; Laser cladding; Hybrid composite coating; lanthanum oxide; H13 tool steel.

1. Introduction

Lasers have already been successfully used in surface engineering to improve the mechanical and electrochemical properties of metals [1)]. Currently, methods such as plasma spraying, arc welding, laser cladding and high-velocity oxy-fuel spray process are used for the deposition of metal-based composite coatings, of which laser technology is increasingly used due to its many advantages such as good coating/substrate bonding, reduction of defects such as porosities, cracks, etc. [2-4)]. The low heat input in this method results in very little mixing of coating and substrate (dilution). It also creates a narrow heat-affected zone, resulting in minimal deformation and warping [5-7)]. Nowadays, laser cladding of hard composite coatings on industrial parts is a common method to increase the wear resistance of the surface [1)]. The application of these coatings leads to an extension of the useful life of parts such as dies, cylinders and rollers that are subject to wear and corrosion [8, 9)].

Nickel-based alloys, because of their good wear and corrosion resistance, are often used in corrosive environments where they are subject to wear and fatigue. However, they do not meet the expected industrial requirements compared to the new coatings that offer better properties, considering that the new applications in industries such as aerospace, oil and gas, etc. require good wear and corrosion resistance at high temperatures. The metal matrix composites are used in many applications such

*Corresponding author
Email: yazdani@sut.ac.ir
Address: Sahand University of Technology, Tabriz, Iran. Tel: +98 41 3345 9456
1.PhD student
2.Professor
3.Professor

as rollers, piston rods, turbines, etc., which require long service life [2, 9, 10]. The addition of ceramic particles such as tungsten carbide, titanium carbide or vanadium carbide into the matrix of a nickel-based alloy leads to better wear performance of the composite coatings. Tungsten carbide is widely used because of its good wettability with nickel and its high hardness [2, 11-16]. Numerous studies have been conducted on the effect of various ceramic particles, especially carbides and oxides, on nickel-based alloys at both room temperature and high temperatures, generally indicating that these particles improve the wear and corrosion resistance of the coatings [15, 17-22]. In addition, the addition of micro/nanoparticles of lanthanide oxides (such as samarium, cerium and yttrium) to the composite coating has been reported to play an important role in increasing wear and corrosion resistance at elevated temperatures [22, 23].

In hybrid composites, known as 2nd generation composites, two or more different particles (in terms of substance or size) are added to the matrix, giving the coating unique properties. They have the potential to be used in various industries such as aerospace, automotive, medical and also to reduce energy consumption. Despite the increasing demand for metal matrix composites, especially aluminum-based ones, which has led to extensive research in this field, there are few studies on the fabrication and characterization of hybrid metal matrix composites. According to the published reports, hybrid metal matrix composites offer comparable or better properties than common metal matrix composites [24-26]. There are reports of improvements in the mechanical properties, especially wear resistance, of aluminium-, titanium- or copper-based hybrid composites, which showed better results compared to simple composites [26-31].

AISI H13 is a chromium, molybdenum and vanadium-containing hot work tool steel with high hardenability and excellent toughness routinely used for the manufacture of dies, extrusion mandrels, plastic moulds, cores, die holder blocks and hot work punches. However, for the majority of hot forming applications such as forging and die casting, both the wear/erosion and corrosion resistance of AISI H13 tool steel at room temperature and elevated temperatures need to be improved. Several studies have used different methods of laser treatment (e.g. cladding, laser hardening) to extend the longevity and save replacement costs. For example, H13 tool steel is ideal for the substrate as it is a commonly used material with high impact strength, wear resistance and ductility for hot forging dies. The steel is pressed under high pressure against the die blanks to form working hubs, which are then used to make working dies called master dies. The working die is shaped to fit into the press in preparation for application. After heat treatment, the material is pressed into the desired shape, resulting in high stress and cyclic fatigue on the die head. During production, the die head must maintain the exact dimensions for the production of the parts. Various coatings have been investigated to improve wear resistance at high temperatures on a variety of high entropy alloys that do not perform well at high temperatures [4]. On the other hand, very few studies have been conducted on metal-based hybrid composites as coatings to extend the life of industrial components. Most studies focused on polymer-based hybrid composites used as biomaterials. Based on this information, we have conducted experiments to optimise the composition and process to extend the lifetime of H13 hot work tool steel.

This work aims to develop a new hybrid composite coating to extend the life of forging and extrusion dies and provide an option for repairing damaged tools. Laser coating of H13 with a nickel-based hybrid composite can provide a cost-effective and more durable option for the industry that is comparable to similar composite coatings.

The microstructure and wear behaviour of H13 hot work tool steel at room temperature and elevated temperature of 700 °C laser coated with 30 wt% tungsten carbide and nickel-based alloy powder and a mixture of lanthanum oxide in the range of 1-4 wt% as a second reinforcement are investigated in this study.

2. Materials and methods

H13 hot work tool steel was used as the substrate with chemical composition given in Table 1. The specimens for the low and high temperature wear tests were cut into disc shapes with a diameter of 30 mm and a thickness of 10 mm and then polished.

Nickel-based superalloy powder (NiCoCrAl) with a particle size of 45-125 μm was used as the material for the matrix of the composite coating. The powder properties are listed in Table 2.

Table 1. Chemical composition of H13 hot work tool steel (wt%).

Element	Fe	C	Si	Mn	Cr	Mo	V
Wt%	Bal.	0.36	0.97	0.23	5.41	1.6	1.17

Table 2. Chemical composition of NiCoCrAl powder (wt%).

Element	Ni	Co	Cr	Al	W
Wt%	36.164	32.178	19.862	9.291	2.505

30 wt% commercial WC-12Co powder (ZHUZHOU Jiangwu Boda) with a particle size of 15-45 μm was added to the matrix powder as carbide reinforcement. According to the results of a similar study, the addition of a higher amount of tungsten carbide (up to 50 wt%) does not have a great influence on the wear resistance [15]. This composition was used as a basis to maintain the toughness of the coating and to evaluate the effects of adding lanthanum oxide in more detail. The lanthanum oxide (Sigma-Aldrich L4000) with purity greater than 99.9% and particle size less than 20 μm was added to the base powder mixture in amounts of 1, 2, 3 and 4 wt%. The scanning electron micrographs of the powders used are shown in Fig.1 (a-c). The prepared powder was mixed in a Turbula mixer for 30 minutes at a speed of 60 rpm. The laser cladding system was equipped with a powder feeder connected to a 400 W pulsed Nd: YAG laser system. The spot diameter was 2 mm and was constant for all samples. Argon was used as shielding and carrier gas with flow rates of 20 L min^{-1} and 15 L min^{-1} respectively.

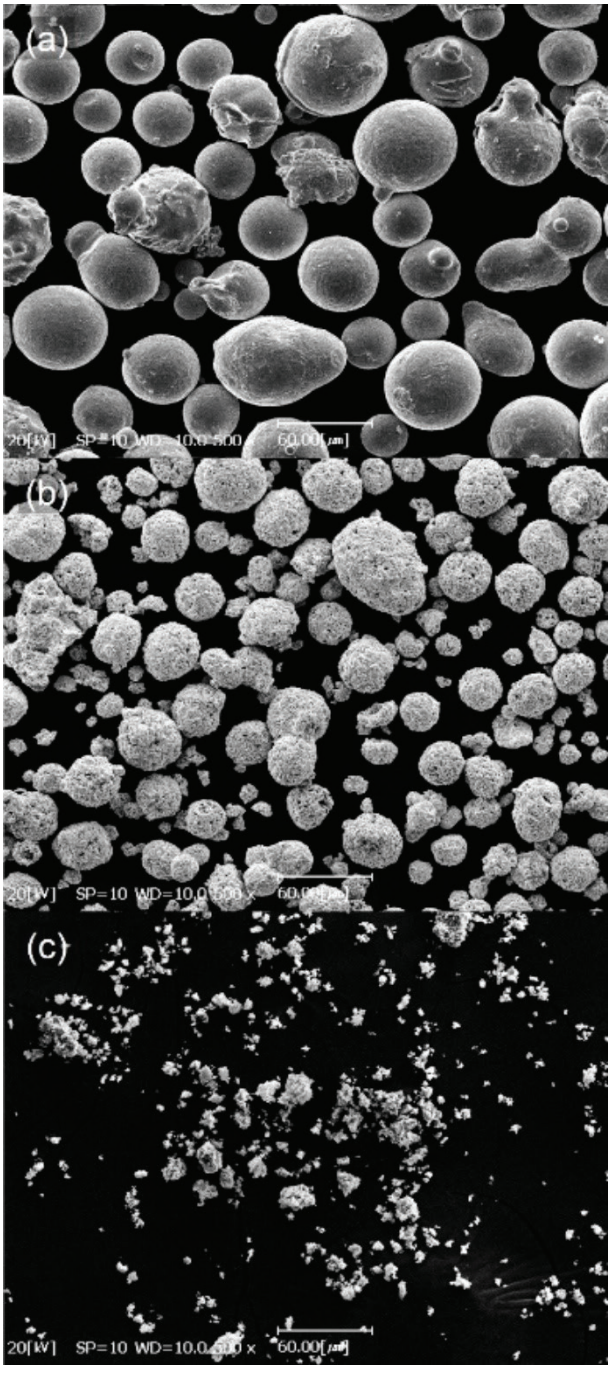

Fig. 1. Scanning electron microscopy images of the powders used for laser cladding of the coatings (a) NiCoCrAl (b) tungsten carbide (c) lanthanum oxide.

The pulse duration and frequency of the Nd: YAG laser were set to 3.5 ms and 35 Hz, respectively. The cladding was performed at a laser power of 300 W, a scanning speed of 3 mm s^{-1}, a powder feed rate of 300 mg s^{-1} and an overlap ratio of 50 %. The total thickness of the coatings after cladding and machining was 150 µm.

A ball-on-disc wear tester (Ducom, India) was used to perform the sliding wear tests on all specimens at both room temperature and 700 °C according to the ASTM G99 standard [23]. An alumina ball with a diameter of 9 mm was used as the abrasive. The applied load and sliding distance were chosen to be 15 N and 200 m, respectively. The wear radius of the coated discs was 12 mm. After the tests, the samples were cleaned with acetone, then dried and weighed with an electronic balance with an accuracy of ±0.1 mg. The wear test was repeated three times for each coating.

Hardness was measured with a Leco M-400-G1 hardness tester at a load of 100 g. Cross-sectional examinations of the cladded coatings as well as the morphology of the coatings, the distribution of ceramic particles and the sliding wear tracks, were assessed using a MIRA3 TESCAN scanning electron microscope. The chemical composition of the claddings was characterised by energy-dispersive X-ray spectroscopy (EDS).

3. Results and discussion

Scanning electron micrographs of the surface of the coating show the distribution of tungsten carbide and lanthanum oxide reinforcer seen as small white particles (Fig. 2 (a-e)). The coatings have the least porosity and defects, which are the advantages of the laser cladding method.

SEM images and maps of the distribution of elements in the cross-section of the coatings are shown in Fig 3.

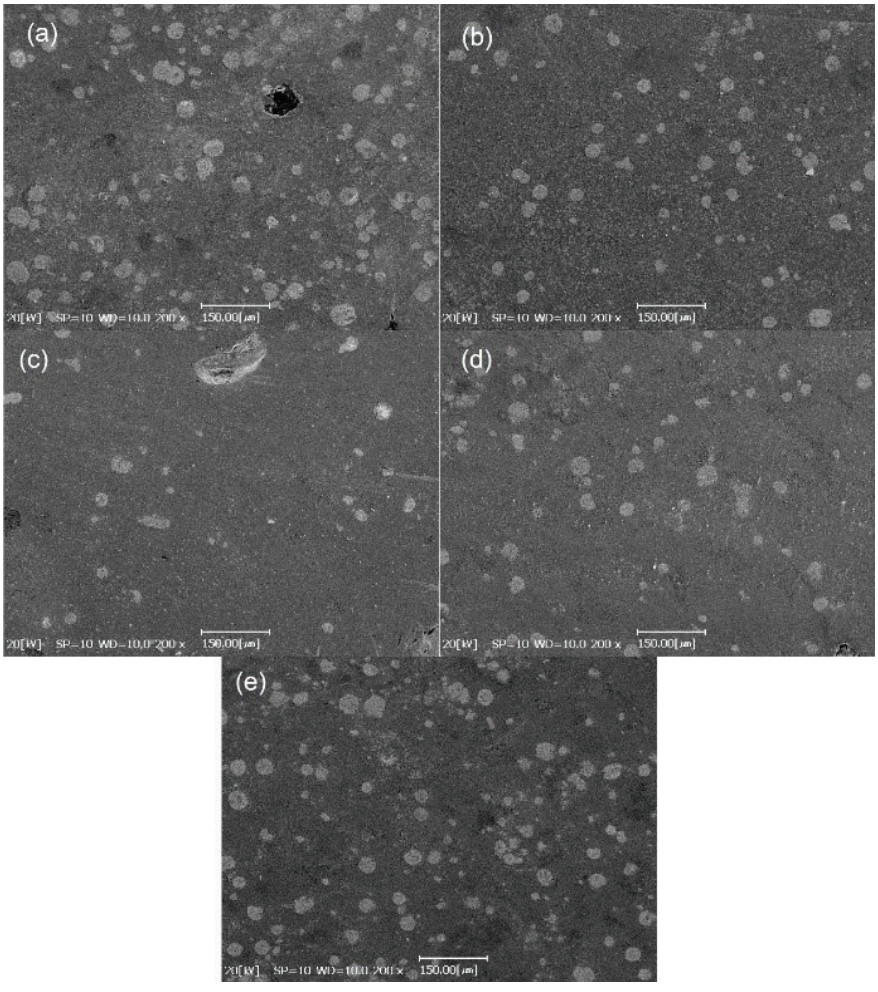

Fig. 2. Scanning electron microscopy images of the coatings surface
(a) NiCoCrAl-30 wt% tungsten carbide-1 wt% lanthanum oxide
(b) NiCoCrAl-30 wt% tungsten carbide-2 wt% lanthanum oxide
(c) NiCoCrAl-30 wt% tungsten carbide-3 wt% lanthanum oxide
(d) NiCoCrAl-30 wt% tungsten carbide-4 wt% lanthanum oxide
(e) NiCoCrAl-30 wt% tungsten carbide.

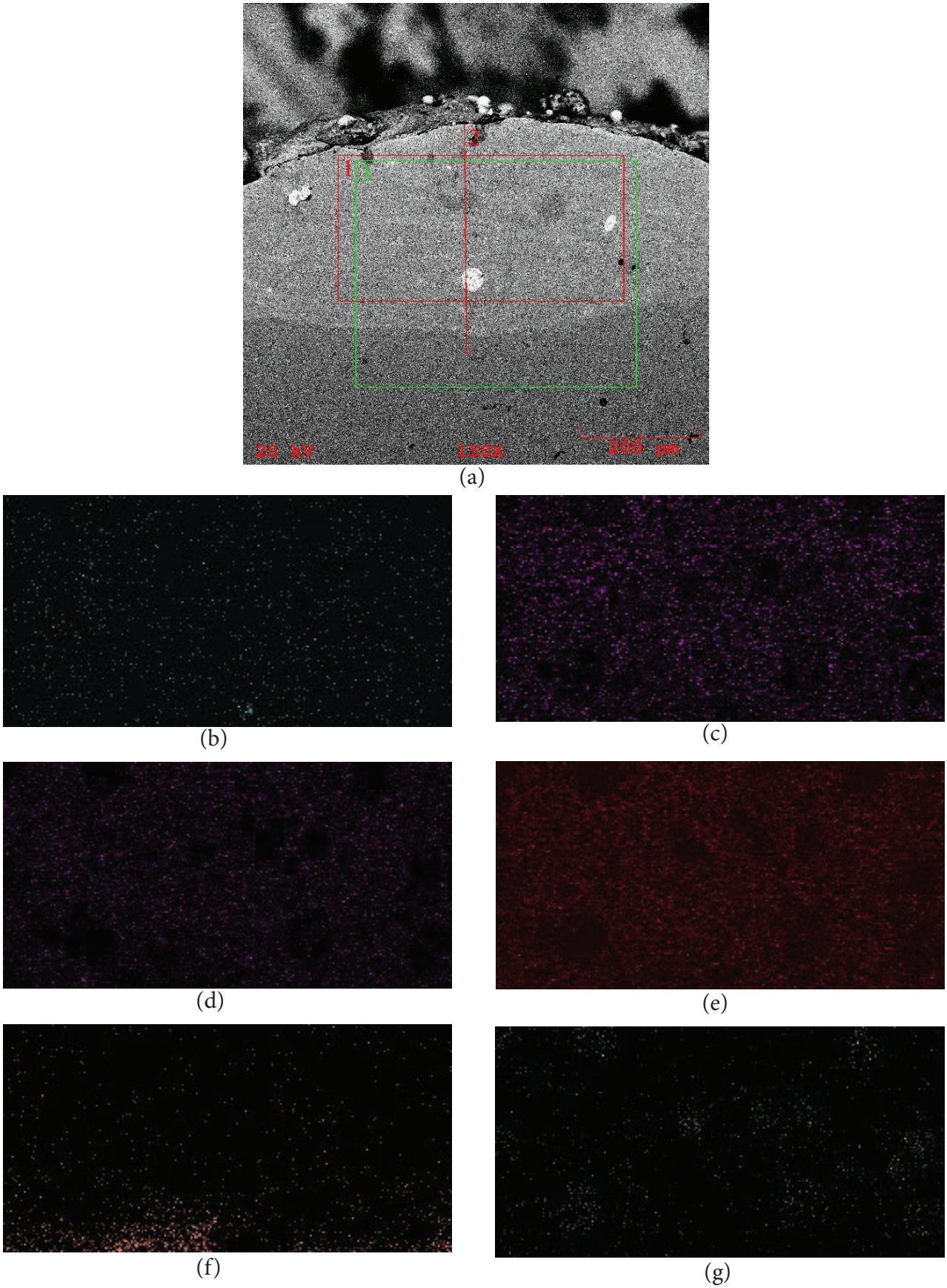

(a)

(b)

(c)

(d)

(e)

(f)

(g)

Fig.3: a) Cross-section SEM images of NiCoCrAl/WC+ 4wt% La_2O_3 coating after 100 h oxidation at 700°C and maps of the distribution of b) La c) Co d) Cr e) Ni f) Fe and g) W in the coating.

3.1. Coatings hardness

The microhardness profile across the cross-section of the coating and substrate shows that the hardness of the substrate is about 300±10 HV0.1, which increases to an average of 518±10 HV0.1 for the sample with the nickel-based alloy (NiCoCrAl) coating, Fig. 4.

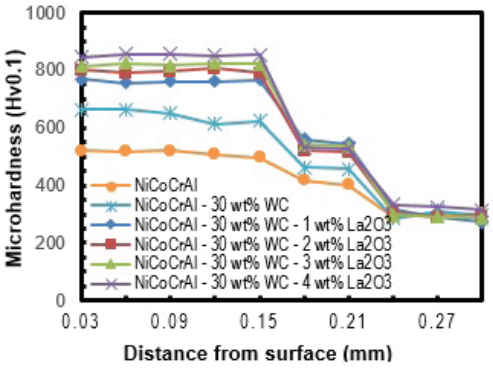

Fig. 4. The variation of microhardness with distance from the surface across the substrate/coatings interface.

For samples with tungsten carbide and lanthanum oxide reinforced particles, the hardness further increased to about 850±10 HV0.1. The increase in hardness is not only due to the rapid solidification during laser cladding, which increases corrosion and wear resistance, but also to the effect of the reinforced particles on the movement of dislocations[32, 33]. Recent research has shown that the addition of lanthanum oxide particles to the matrix increases the oxidation resistance of the coating at high temperatures and increases hardness [22, 23]. The changes in hardness can be explained by the fact that lanthanum oxide particles with uniform distribution contribute to the increase of heterogeneous nucleation sites in the melt, which subsequently leads to fine dendrites and equiaxed grains [21], where the structure of two coatings is compared, Fig. 5.

It should be noted that due to the high melting point of lanthanum oxide (2315 °C) and the rapid solidification, the particles remained in the melt in solid form. It is assumed that the drop in hardness in the intersection is caused by the dilution effect resulting from the partial

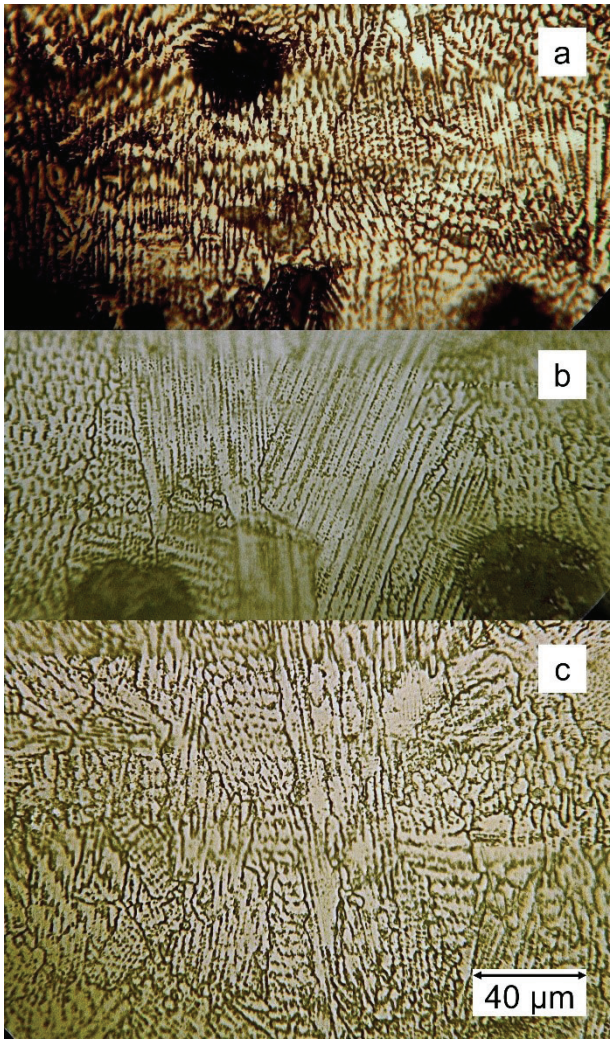

Fig. 5. Optical microscopy images of cross section of coatings a) NiCoCrAl-30wt% WC –2wt%La_2O_3 , b) NiCoCrAl-30wt% WC and c) NiCoCrAl (×1000).

melting of the substrate. Since the coating formed very quickly and the coefficients of thermal expansion of the coating and the substrate are different, residual stresses are created in the coating. The residual stresses, together with the gradual decrease in hardness at the interface between the coating and the substrate, increase the adhesion and reduce the brittleness of the coating, which is considered to be an advantage that could protect it from cracking [32].

3.2. Wear behaviour at room temperature

The densities of NiCoCrAl, tungsten carbide and lanthanum oxide were determined by the Archimedean method to be 7.38, 15.59 and 6.46 gr cm^{-3}, respectively. Accordingly, the density of the coatings is calculated using the composite density formula given in equation 1 [34]. The results are shown in Table 3 together with the weight loss of each coating during the wear test.

$$\left({}^{1}/_{\rho_{composite}}\right) = \left({}^{X_i}/_{\rho_i}\right) + \left({}^{X_j}/_{\rho_j}\right) + \left({}^{X_k}/_{\rho_k}\right) \quad \text{Eq. (1)}$$

Due to the differences in density and composition of the coatings, the amount of weight loss in the wear test may not be a good criterion for evaluating wear resistance. Therefore, a unique criterion was used to calculate the wear rate according to equation 2 [34].

$$WR = {}^{m}/_{\rho FL} \quad \text{Eq. (2)}$$

where WR is the wear rate (mm^3 N m), m is the average mass loss (mg), F is the applied force (N), L is the sliding distance (m) and ρ is the density of the materials (g cm^{-3}). The results of these calculations show that adding reinforced particles to the coating decreases the wear rate by 2.5 to 3.5 times (Fig. 6).

Table 3. Density and weight loss of coatings.

Coating	Density (g cm^{-3})	weight loss (mg)
NiCoCrAl	7.38	5.6
NiCoCrAl-30 wt% tungsten carbide	8.77	2.6
NiCoCrAl-30 wt% tungsten carbide-1 wt% lanthanum oxide	8.75	2
NiCoCrAl-30 wt% tungsten carbide-2 wt% lanthanum oxide	8.73	1.9
NiCoCrAl-30 wt% tungsten carbide-3 wt% lanthanum oxide	8.72	2.2
NiCoCrAl-30 wt% tungsten carbide-4 wt% lanthanum oxide	8.70	2.6

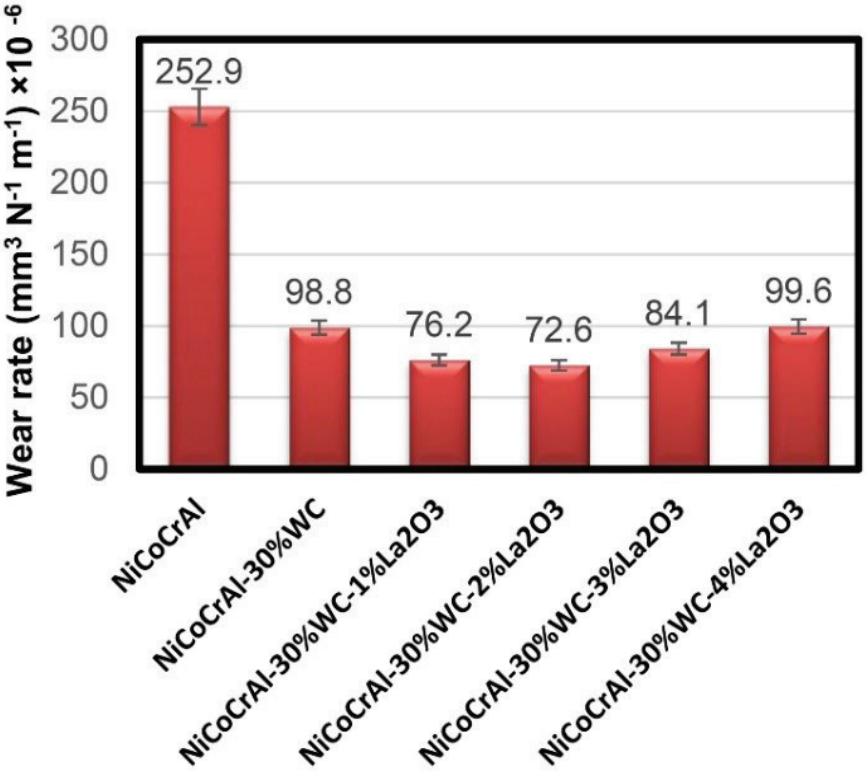

Fig. 6. Wear rate of the coatings as obtained from the ball-on-disc wear test.

The wear rate is significantly reduced by the addition of 1-3 wt% lanthanum oxide, with the minimum rate in the coating being achieved at an amount of 2 wt% lanthanum oxide. The reason for this could be the uniform distribution of the particles, which leads to the formation of equiaxed grains. Moreover, the high hardness of the coating is a reason for the good wear resistance according to the relationship between hardness and wear resistance explained by Archard's equation [35, 36]. However, the increase in wear rate for the coating with 4 wt% lanthanum oxide is due to the high hardness and the resulting brittleness of the coating. In addition, the increased number of obstacles against dislocations could be the source of microcracks. A microcrack forms near a lanthanum oxide particle and it can be assumed that the strong plastic deformation around two lanthanum oxide particles is responsible for the crack formation, Fig. 7.

The variation of the coefficient of friction with sliding distance and the scanning electron micrographs of the worn surfaces show that the coefficient of friction varies in the range of 0.54 to 0.72, Figs. 8 and 9 a-f.

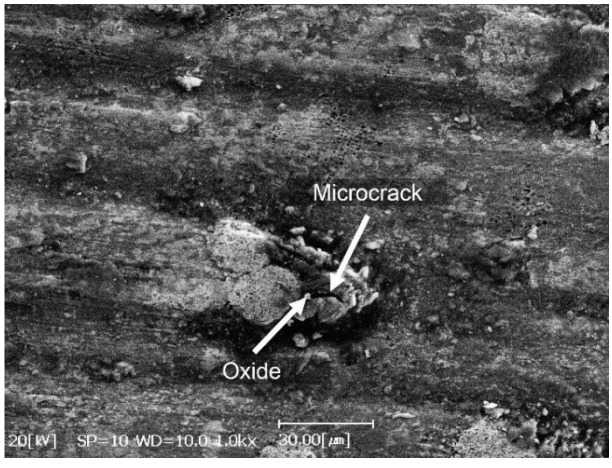

Elt.	Line	Intensity (c/s)	Conc	Units	Error 2-sig	MDL 3-sig
C	Ka	0.84	0.931	wt.%	46.940	1.590
O	Ka	5.60	4.428	wt.%	13.665	0.296
Al	Ka	2.43	1.386	wt.%	14.784	0.312
Cr	Ka	7.46	3.754	wt.%	13.021	0.720
Fe	Ka	6.50	4.542	wt.%	20.727	0.499
Co	Ka	3.38	2.663	wt.%	15.497	0.511
Ni	Ka	2.46	2.112	wt.%	16.552	0.682
La	La	66.82	63.726	wt.%	0.406	1.311
W	La	5.53	16.458	wt.%	5.971	2.417
			100.000	wt.%		Total

kV 20.0
Takeoff Angle 45.0°
Elapsed Livetime 30.0

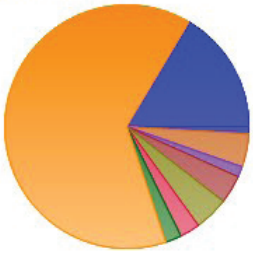

Fig. 7: (a) Scanning electron microscopy image indicating a microcrack beside a lanthanum oxide particle on the worn surface of NiCoCrAl-30 wt% tungsten carbide-4 wt% lanthanum oxide coating and (b) energy dispersive X-ray spectroscopy result for oxide particle.

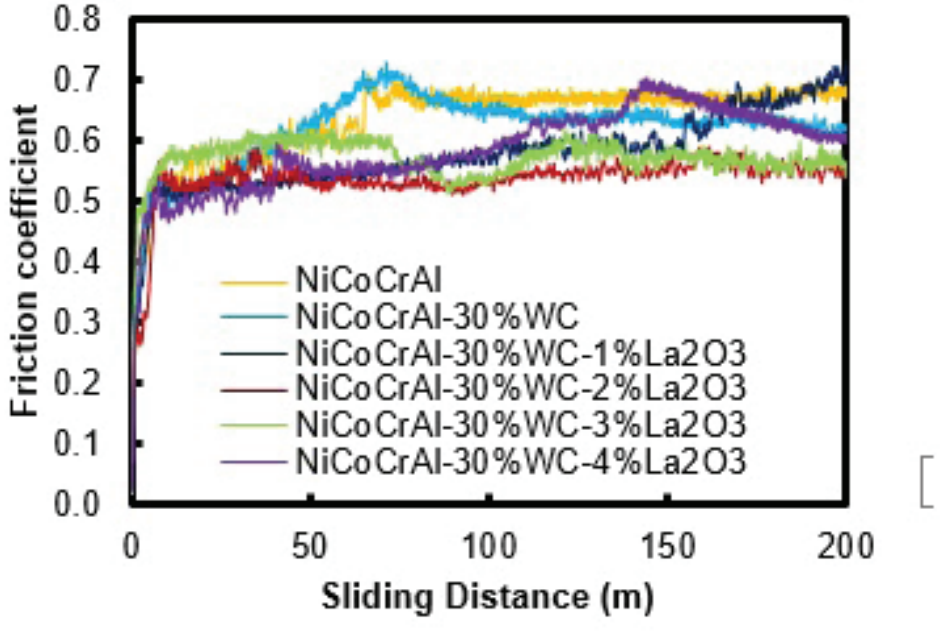

Fig. 8. Variation of friction coefficients with sliding distance at room temperature for coatings.

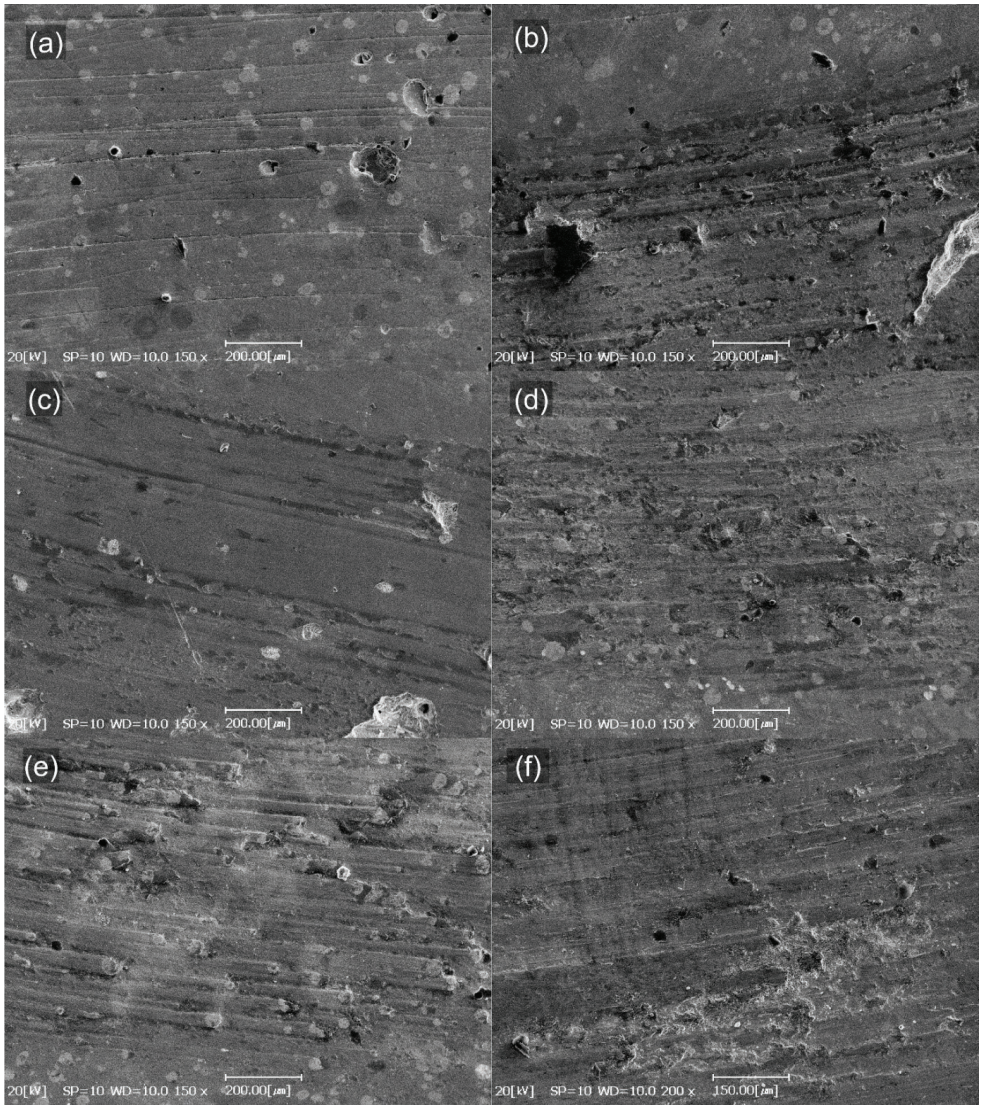

Fig. 9. Scanning electron microscopy images of the wear tracks at room temperature for
(a) NiCoCrAl-30 wt% tungsten carbide-1 wt% lanthanum oxide
(b) NiCoCrAl-30 wt% tungsten carbide-2 wt% lanthanum oxide
(c) NiCoCrAl-30 wt% tungsten carbide-3 wt% lanthanum oxide
(d) NiCoCrAl-30 wt% tungsten carbide-4 wt% lanthanum oxide
(e) NiCoCrAl-30 wt% tungsten carbide and
(f) NiCoCrAl coatings.

For the samples containing 1-3 wt% lanthanum oxide, the variation of the coefficient of friction is smaller than for the others and a uniform sliding over a distance of 10 m starts. The coefficient of friction of the coating with 4 wt% lanthanum oxide is very variable and fluctuated during the test, which is due to the cracks, as explained above. The coefficient of friction of NiCoCrAl-30 wt% tungsten carbide and NiCoCrAl coatings reaches a steady state after a sliding distance of 100 and 70 m, respectively. For the sample with 1 wt% lanthanum oxide, the coefficient of friction increases in the last 50 m of the sliding distance, which could be due to the detachment of the reinforced particles, which further affects the wear process (Fig. 8). The detachment of the reinforced particles can be observed. The grooves on the worn surface are indicative of abrasive wear, Fig. 9. When coated with 2 wt% lanthanum oxide, the increase in hardness reduces the width of the wear marks, Fig. 9b [37]. Lamellar removal of debris from the worn surface can also be seen, Fig. 9f. Some explanations have been proposed, e.g. that the compressive stress at the surface causes the cracking by plastic shear deformation under the worn surface[38]. However, it appears that the dislocation aggregations in the wear substrate are more acceptable to the alloy coating without reinforced particles. Accordingly, the dislocations are aggregated and interconnected under the

surface during wear, and eventually, cavities are formed below the surface. These cavities gradually become more numerous and join together to form cracks along with the surface. The cracks become larger and reach a critical size by which the materials are removed from the surface in a lamellar manner [2, 3, 38, 39]. Some of these cavities can be observed in Fig. 10.

3.3. High-temperature friction and wear behaviour of coatings

The variations of the coefficient of friction of laser cladded coatings with the sliding distance (Alumina ball counterpart; sliding velocity: 0.1 m s^{-1}, temperature: 700 °C) are shown in Fig. 11 a-f.

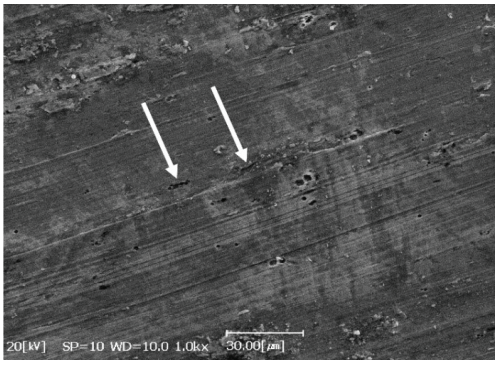

Fig. 10. Scanning electron microscopy image of from the worn surface of NiCoCrAl coating indicating the holes (shown by arrows) created by dislocations aggregation.

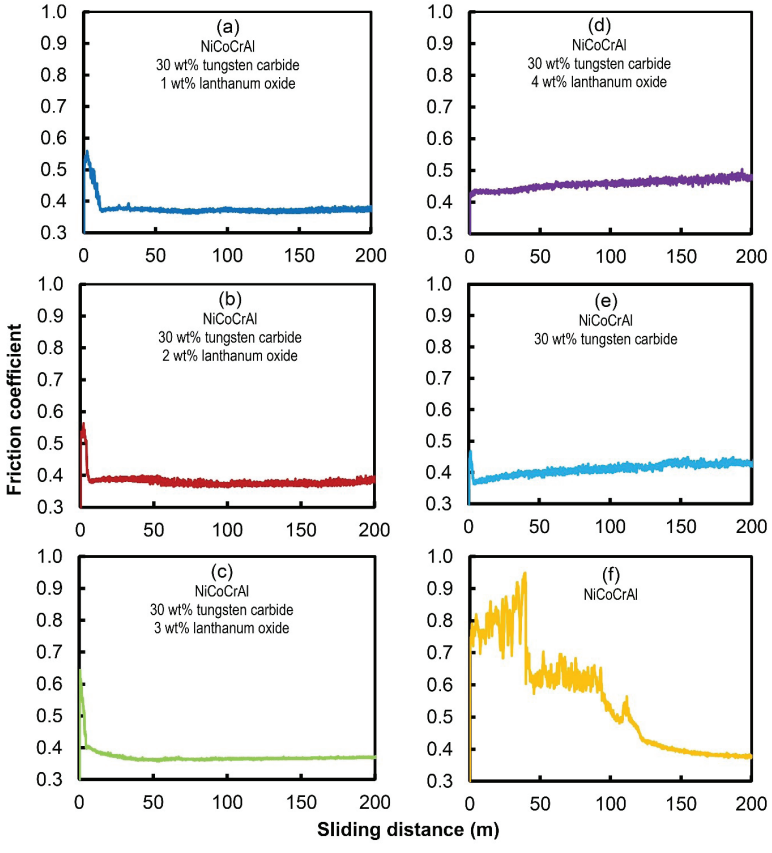

Fig. 11. Variation of friction coefficient with sliding distance at 700 °C for coatings:
(a) NiCoCrAl-30 wt% tungsten carbide-1 wt% lanthanum oxide
(b) NiCoCrAl-30 wt% tungsten carbide-2 wt% lanthanum oxide
(c) NiCoCrAl-30 wt% tungsten carbide-3 wt% lanthanum oxide
(d) NiCoCrAl-30 wt% tungsten carbide-4 wt% lanthanum oxide
(e) NiCoCrAl-30 wt% tungsten carbide
(f) NiCoCrAl.

As can be seen, the coatings with 1-3 wt% of lanthanum oxide have achieved a constant coefficient of friction at short sliding distances of about 10 to 25 m. The coefficient of friction of the coatings with 1 to 3 wt% of lanthanum oxide has been shown in Fig. 11 a-f. The coefficients of friction range from 0.37 to 0.39, which is the lowest compared to the other coatings, indicating improved wear resistance, Fig. 11 a-c. For the coating with 2 wt% lanthanum oxide, the steady-state of friction starts earlier due to the dense and uniform microstructure and high hardness [40]. The friction coefficient of the sample with 4 wt% lanthanum oxide increased with a small slope, which can be attributed to the separation of worn debris that subsequently causes three-body abrasion. The coefficient of friction of the coating without reinforced particles shows many variations during the test, indicating adhesive wear as the dominant mechanism [37]. In the last 30 m of the wear track, the coefficient of friction has reached a constant value of 0.39, indicating that the wear mechanism has changed to abrasive wear.

The scanning electron micrographs of the wear marks on the coatings are shown in Fig. 12 a-f. The dominant mechanism for all coatings, including the sample with lanthanum oxide, is abrasive wear, Fig. 12 a-d.

The coating without reinforced particles was subjected to a combination of adhesive and abrasive wear.

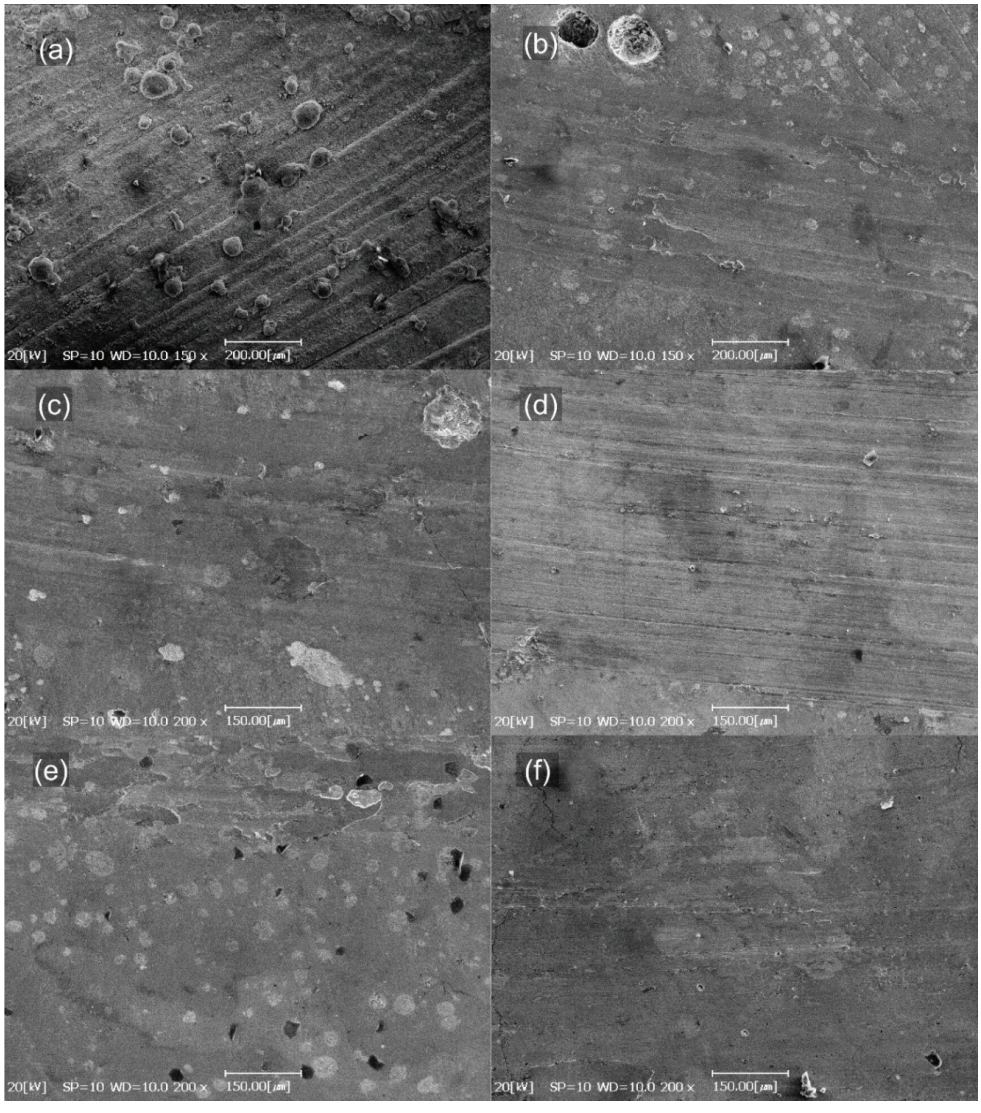

Fig. 12. Scanning electron microscopy images of the wear tracks at 700 °C for
(a) NiCoCrAl-30 wt% tungsten carbide-1 wt% lanthanum oxide
(b) NiCoCrAl-30 wt% tungsten carbide-2 wt% lanthanum oxide
(c) NiCoCrAl-30 wt% tungsten carbide-3 wt% lanthanum oxide
(d) NiCoCrAl-30 wt% tungsten carbide-4 wt% lanthanum oxide
(e) NiCoCrAl-30 wt% tungsten carbide and
(f) NiCoCrAl coatings.

For the NiCoCrAl-30 wt% tungsten carbide coating, the particles detached and the wear mechanism was adhesive. The detached particles subsequently acted as abrasive particles and resulted in intense three-body abrasive wear, which increased the friction coefficient of the composite coating. A uniform distribution of the lanthanum oxide particles reduces this effect and prevents the particles from detaching [40].

It can be seen that the grooves in the sample with 4 wt% lanthanum oxide are deeper than in the others. Less wide wear scars are seen in the samples with 2 and 3 wt% lanthanum oxide than in the sample with 1 wt% lanthanum oxide. The higher hardness is the reason for the smaller width of the wear scars, but the coating has shown a different behaviour, Fig. 12a. For a more detailed investigation, energy dispersive X-ray spectroscopy was performed on the wear marks of the three coatings. The analysis for three regions of the 1 wt% lanthanum oxide coating is shown in Fig. 13.

Analysis of these three regions indicates the presence of oxygen, which was not detected in the other coatings, Fig. 13 a-d. It has been reported that when chromium is increased up to 33 wt%, the presence of 1 wt% lanthanum oxide accelerates the diffusion of chromium to the surface, leading to the formation of chromium oxide [63]. The oxide residues were detected in region 2, Fig. 13 a. Energy-dispersive X-ray spectroscopy of the coating with 4 wt% lanthanum oxide is shown in Fig. 14.

It can be observed that the iron concentration in the worn region is high (54.7 wt%), indicating that the grooves are so deep that the coating has been worn down to the dilution region. The reason for the low wear resistance of this coating could be related to the high number of lanthanum oxide particles that act as dislocation barriers and cause the separation of debris. These debris

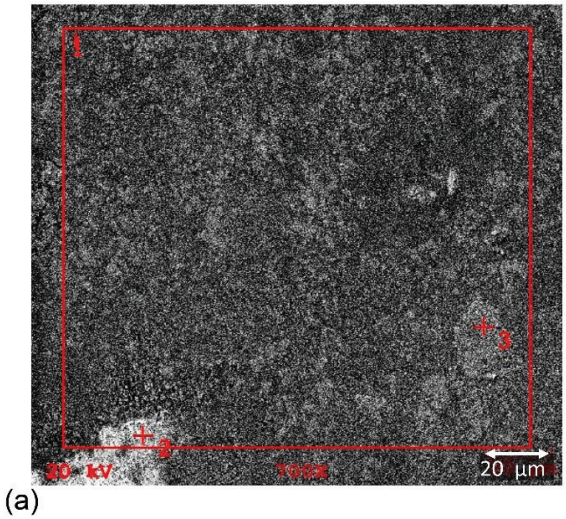

(a)

Element	Line	Intensity (c/s)	Concentration wt%	Error 2-Sig	MDL 3-Sig
C	kα	1.22	1.123	45.757	1.617
O	kα	18.10	6.005	7.759	0.417
Al	kα	33.24	6.456	3.808	0.325
Cr	kα	93.22	19.393	1.972	0.312
Fe	kα	10.20	2.439	8.114	0.351
Co	kα	96.59	27.840	1.939	0.432
Ni	kα	67.32	21.545	2.466	0.470
W	Lα	14.35	17.199	5.079	2.076

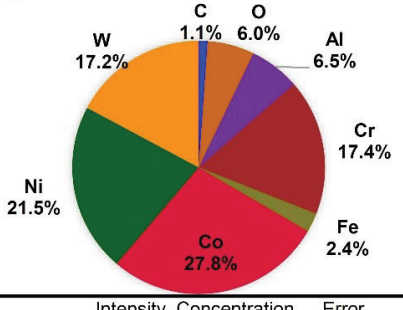

(b)

Element	Line	Intensity (c/s)	Concentration wt%	Error 2-Sig	MDL 3-Sig
C	kα	0.63	0.552	68.224	1.320
O	kα	13.30	4.248	9.355	0.294
Al	kα	18.38	3.738	5.297	0.287
Cr	kα	167.43	32.858	1.400	0.291
Fe	kα	9.37	2.426	8.380	0.345
Co	kα	77.69	23.803	2.155	0.397
Ni	kα	51.95	17.610	2.821	0.418
W	Lα	11.82	14.765	5.220	1.849

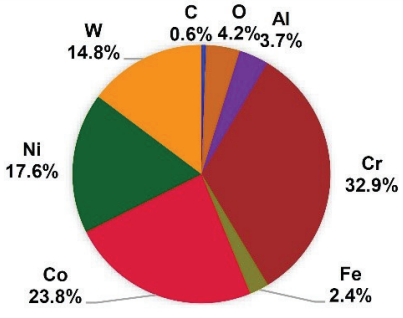

(c)

Element	Line	Intensity (c/s)	Concentration wt%	Error 2-Sig	MDL 3-Sig
C	kα	0.54	0.430	97.300	1.394
O	kα	28.87	13.325	5.534	0.621
Al	kα	16.86	2.526	6.707	0.331
Cr	kα	60.20	12.858	2.643	0.405
Fe	kα	3.00	0.776	24.795	0.447
Co	kα	17.12	4.989	5.945	0.500
Ni	kα	7.12	2.224	13.221	0.582
W	Lα	52.69	62.871	2.150	1.798

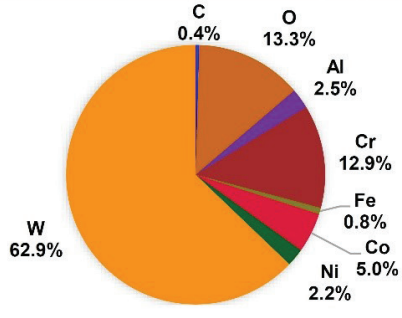

(d)

Fig. 13. (a) Scanning electron microscopy image of worn surface indicating region and points of energy-dispersive X-ray spectroscopy of coating with 1 wt% lanthanum oxide. The energy-dispersive X-ray spectroscopy results for (b) region 1 (c) point 2 and (d) point 3.

behave like abrasive particles and cause severe wear [40-44].

A scanning electron micrograph of the wear marks on the coating without reinforced particles is shown in Fig. 15a.

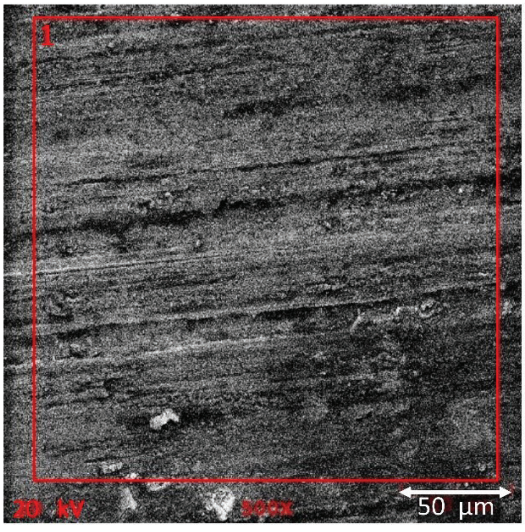

(a)

Element	Line	Intensity (c/s)	Concentration wt%	Error 2-Sig	MDL 3-Sig
C	k_α	0.67	0.694	92.959	1.764
O	k_α	6.51	1.705	11.616	0.395
Al	k_α	56.39	12.167	2.656	0.310
Cr	k_α	2.88	0.759	27.673	0.353
Fe	k_α	177.36	54.701	1.379	0.436
Co	k_α	31.01	11.928	3.895	0.487
Ni	k_α	20.08	8.607	4.842	0.507
W	L_α	6.22	9.437	7.751	1.883

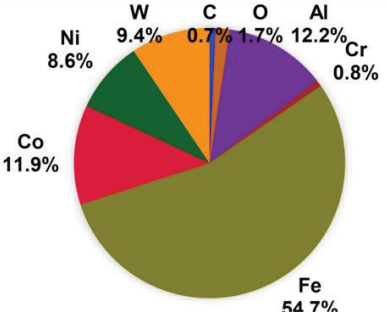

(b)

Fig. 14. (a) Scanning electron microscopy image of coating with 4 wt% lanthanum oxide worn surface (b) energy dispersive X-ray spectroscopy result for region 1.

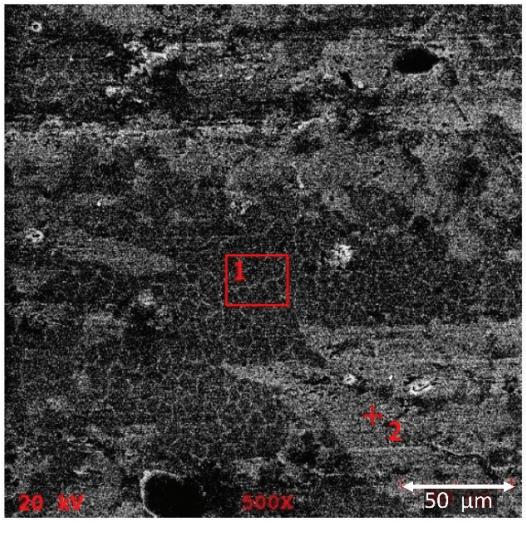

(a)

Element	Line	Intensity (c/s)	Concentration wt%	Error 2-Sig	MDL 3-Sig
C	k_α	0.77	0.704	70.894	1.555
O	k_α	48.22	9.171	3.006	0.294
Al	k_α	135.12	21.679	1.582	0.249
Cr	k_α	4.16	0.874	15.259	0.277
Fe	k_α	135.70	35.193	1.578	0.314
Co	k_α	98.92	28.653	1.916	0.351
Ni	k_α	3.44	3.726	12.268	1.136
W	L_α	0.77	0.704	70.894	1.555

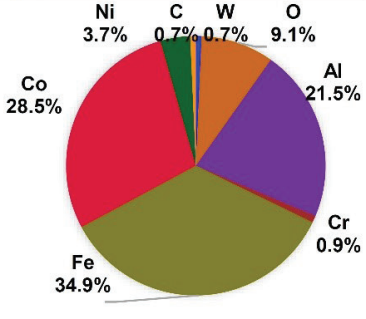

(b)

Element	Line	Intensity (c/s)	Concentration wt%	Error 2-Sig	MDL 3-Sig
C	k_α	0.84	0.801	73.707	1.698
O	k_α	49.30	9.707	2.842	0.247
Al	k_α	126.47	20.753	1.627	0.232
Cr	k_α	4.79	1.019	14.427	0.301
Fe	k_α	120.35	31.958	1.708	0.385
Co	k_α	111.15	33.041	1.796	0.409
Ni	k_α	2.45	2.721	15.965	1.219
W	L_α	0.84	0.801	73.707	1.698

(c)

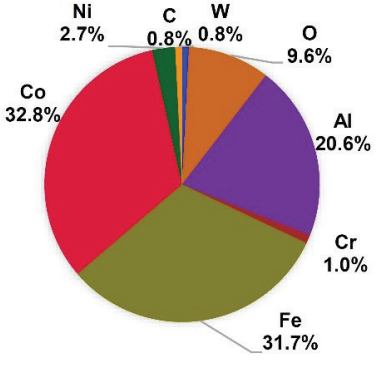

Fig. 15. (a) Scanning electron microscopy image of worn surface indicating points of energy-dispersive X-ray spectroscopy of NiCoCrAl coating. The energy-dispersive X-ray spectroscopy results for (b) point 1 and (c) point 2.

The wear grooves are not visible in the image. Two distinct regions can be observed, labelled 1 and 2. Energy-dispersive X-ray spectroscopy analysis of regions 1 and 2 shows that there are no significant chemical differences in these regions, Fig. 15b and 15c. Consequently, the predominant mechanism in the coating is adhesive wear, Fig. 10f. The lower hardness of this coating compared to the other coatings causes the temperature on the softer coating to rise, so that some parts of the surface stick to the ball and detach from the sample when the alumina sphere wears away [39].

4. Conclusions

By investigating the effects of the addition of lanthanum oxide particles in laser cladded NiCoCrAl/tungsten carbide hybrid composite coating on the wear behaviour, the following conclusions can be drawn.

By applying the wear-resistant NiCoCrAl alloy coating, the base hardness increased from about 300±10 HV0.1 to an average of 518 HV0.1. By adding tungsten carbide and lanthanum oxide reinforced particles, the hardness further increased to about 850±10 HV0.1.

The addition of 1-3 wt% lanthanum oxide to the coating significantly reduced the wear rate at room temperature. The lowest wear rate was observed in the sample with 2 wt% lanthanum oxide. This behaviour was associated with the high hardness of the coating, the uniform distribution of the particles and the formation of equiaxed grains, which consequently resulted in a homogeneous microstructure in the coating. However, when coated with 4 wt% lanthanum oxide, an increase in the wear rate was observed. This could be due to the high hardness and the resulting brittleness of the coating. In addition, the increased number of obstacles against dislocations could be the source of microcracks.

Microscopic examination of the wear marks on the coatings showed that the wear mechanism for all coatings was abrasive wear. However, lamellar detachment was observed in the coatings without reinforced particles. This is related to the aggregation of dislocations under the surface, which led to the formation of cavities. These cavities gradually increased in size and coalesced into cracks along the surface. The cracks became larger and reached a critical size, separating the wear layers from the surface. The measured coefficient of friction as a function of sliding distance confirms these results.

The results of the wear test at 700 °C showed that the addition of lanthanum oxide changed the wear mechanism from adhesive to abrasive wear. However, when more than 3 wt.% lanthanum oxide was added, there was severe wear of the coating due to the detaching deposits.

5. Acknowledgements

The authors would like to thank Sahand University of Technology, Tabriz, Iran, for supporting this research and providing laboratory facilities. P.A. would like to thank Dr Mohsen GolzarShahri (Isfahan University of Technology) for the scanning electron microscopic analysis and his tireless help.

Reference

[1] K. Wang, B. Chang, Y. Lei, H. Fu, Y. Lin: Metals, 2017, 7 (12), 551.

[2] K. Wang, D. Du, G. Liu, B. Chang, Y. Hong: Sci. Technol. Weld. Joining, 2019, 24 (5), 517.

[3] J. Zhang, X. Guo, Y. Zhang, Z. Lu, H.-H. Choi, Y.-G. Jung, I.-S. Kim: Adv. Appl. Ceram., 2019, 118 (5), 257.

[4] M.T. Wall, M.V. Pantawane, S. Joshi, F. Gantz, N.A. Ley, R. Mayer, A. Spires, M.L. Young, N. Dahotre: Surf. Coat. Technol., 2020, 387, 125473.

[5] E. Toyserkani, A. Khajepour, S.F. Corbin: Laser cladding, CRC press, Boca Raton 2004.

[6] A. Frenk, M. Vandyoussefi, J.D. Wagnière, W. Kurz, A. Zryd: Metall. Mater. Trans. B, 1997, 28 (3), 501.

[7] Y. Hu, C. Chen, K. Mukherjee: J. Mater. Sci., 1998, 33 (5), 1287.

[8] H. Wang, W. Zhang, Y. Peng, M. Zhang, S. Liu, Y. Liu: Coatings, 2020, 10 (3), 300.

[9] S.R. Al-Sayed Ali, A.H.A. Hussein, A.A.M.S. Nofal, S.E.I. Hasseb Elnaby, H.A. Elgazzar, H.A. Sabour: Materials, 2017, 10 (10), 1178.

[10] S. Ghanbari, F. Mahboubi: Mater. Des., 2011, 32 (4), 1859.

[11] J. Jiang, Y. Sun, Y. Chen, Q. Zhou, H. Rong, X. Hu, H. Chen, L. Zhu, S. Han: Surf. Eng., 2020, 36 (8), 889.

[12] M.C. Sahour, A. Bahloul, A.B. Vannes: Int. J. Mater. Form., 2008, 1 (1), 1379.

[13] C. Guo, J. Zhou, J. Zhao, L. Wang, Y. Yu, J. Chen, H. Zhou: Tribol. Lett., 2011, 44 (2), 187.

[14] G.Y. Liang, T.T. Wong: J. Mater. Eng. Perform., 1997, 6 (1), 41.

[15] J. Nurminen, J. Näkki, P. Vuoristo: Int. J. Refract. Met. Hard Mater., 2009, 27 (2), 472.

[16] B.M. Dhakar, D.K. Dwivedi, S.P. Sharma: Surf. Eng., 2012, 28 (1), 73.

[17] C. Pan, H. Wang, H. Wang, Q. Chang, H. Wang: J. Wuhan Univ. Technol., Mater. Sci. Ed., 2010, 25 (6), 991.

[18] H.-Y. Wang, D.-W. Zuo, M.-D. Wang, G.-F. Sun, M. Hong, Y.-L. Sun: Trans. Nonferrous Met. Soc. China, 2011, 21 (6), 1322.

[19] B. He, D. Ma, F. Ma, K. Xu: Ferroelectrics, 2019, 547 (1), 217.

[20] J. Li, Z.-s. Yu, H.-p. Wang, M.-p. Li: Int. J Min. Met. Mater., 2010, 17 (4), 481.

[21] S.H. Zhang, M.X. Li, J.H. Yoon, T.Y. Cho: Mater. Chem. Phys., 2008, 112 (2), 668.

[22] D. Shu, X. Cui, Z. Li, J. Sun, J. Wang, X. Chen, S. Dai, W. Si: Metals, 2020, 10 (3), 383.

[23] M. Omidi, M. Yeganeh, A. Etemad, M. Rostami, M. Shafie:

Journal of Advanced Materials and Processing, 7(2019), 3.
[24] L. Prasad, A. Saini, V. Kumar: J. Nat. Fibers, 2019, 1.
[25] S.M. Maharana, A.K. Pradhan, M.K. Pandit: J. Nat. Fibers, 2020, 1.
[26] A.H. Makwana, A. Shaikh: J Adhes., 2019,
[27] A. Swain, T. Roy, B.K. Nanda: Mech. Adv. Mater. Struct., 2017, 24 (2), 95.
[28] S. Aliyeva, A. Maharramov, A. Azizov, R. Alosmanov, I. Buniyatzadeh, G. Eyvazova: Anal. Lett., 2016, 49 (14), 2347.
[29] M. Ali, K. Alam, Y. Al-Majali, M. Kennedy: J. Air Waste Manage. Assoc., 2017, 67 (9), 1036.
[30] M. Maghsoudi-Ganjeh, L. Lin, X. Wang, X. Zeng: Int. J Smart Nano Mater., 2019, 10 (1), 90.
[31] K. Ushashri, M. Masanta: Mater. Manuf. Processes, 2015, 30 (6), 730.
[32] F. Madadi, F. Ashrafizadeh, M. Shamanian: J. Alloys Compd., 2012, 510 (1), 71.
[33] D. Hritcu, G. Dodi, M.L. Iordache, D. Draganescu, E. Sava, M.I. Popa: Appl. Surf. Sci., 2016, 387, 332.
[34] S. Paydar, A. Jafari, M.E. Bahrololoom, V. Mozafari: Tribol.-Mater., Surf. Interfaces, 2015, 9 (2), 105.
[35] J.C. Ion: Laser processing of engineering materials: principles, procedure and industrial application, Elsevier Butterworth-Heinemann, Oxford 2005.
[36] I. Hemmati, V. Ocelik, J.T.M. De Hosson: J. Mater. Sci., 2011, 46 (10), 3405.
[37] F. Zhou, H. Zhang, C. Sun, J. Dai: Surf. Eng., 2019, 35 (8), 683.
[38] A. Bigos, E. Beltowska-Lehman, E. García-Lecina, M. Bieda, M.J. Szczerba, J. Morgiel: J. Alloys Compd., 2017, 726, 410.
[39] A. Rezaeiolum, M. Aliofkhazraei, A. Karimzadeh, A.S. Rouhaghdam, R. Miresmaeili: Surf. Eng., 2018, 34 (6), 423.
[40] N.P. Wasekar, G. Sundararajan: Wear, 2015, 342-343, 340.
[41] G. Singh, M. Kaur: Surf. Eng., 2020, 36 (11), 1139.
[42] J. Nasehi, H.M. Ghasemi, M. Abedini: Tribol. Trans., 2016, 59 (2), 286.
[43] X. Ren, Z. Tong, W. Zhou, L. Chen, Y. Ren, F. Dai, Y. Ye, S. Adu-Gyamfi, J. Yang, L. Li: Mater. Sci. Technol., 2018, 34 (18), 2294.
[44] K. Zhang, J. Liu, B. Bao, H. Xu: Surf. Interface Anal., 2018, 50 (4), 448.